

## Sulfur $L_{2,3}$ and zinc $M_{2,3}$ soft-x-ray fluorescence spectra in CdS and ZnS

L. Zhou, T. A. Callcott, and J. J. Jia  
*University of Tennessee, Knoxville, Tennessee 37996*

D. L. Ederer  
*Tulane University, New Orleans, Louisiana 70118*

Rupert Perera  
*Lawrence Berkeley Laboratory, Berkeley, California 94720*  
 (Received 24 May 1996)

The sulfur  $L_{2,3}$  soft-x-ray emission spectra of wurtzite CdS and cubic ZnS and the zinc  $M_{2,3}$  spectra of ZnS have been measured using both photon and electron-beam excitation. The photon-excited sulfur  $L$  spectra are found to be much sharper than electron-beam-excited spectra. Using photon excitation between the  $L_2$  and  $L_3$  thresholds, a pure  $L_3$  spectrum is obtained for both materials. Broad features of the S  $L$  spectra, consisting of a lower valence band (LVB) derived from the sulfur  $3s$  orbital and an upper valence band (UVB) derived from S  $3p$  and Cd(Zn)  $s$  and  $p$  orbitals, are typical of materials with mixed ionic-covalent character. A narrow band between the UVB and LVB is associated with overlap of Zn  $3d$  and Cd  $4d$  orbitals onto the S site. The  $s+d$  local partial density of states derived from these spectra provide a rigorous test of band-structure calculations; they are in good agreement for the position, width, and structure of the LVB and UVB, but place the  $d$  band deeper in the subband gap than theory predicts. The Zn  $M_{2,3}$  spectrum has large lifetime broadening and thus provides limited information. However, near-threshold excitation of this spectrum shows dramatic effects resulting from an electronic resonance Raman process. [S0163-1829(97)02208-X]

### I. INTRODUCTION

The II-VI sulfur compounds CdS and ZnS and related semiconductor alloys have important applications in modern science and technology. For example, light-emitting diodes utilizing  $\text{ZnS}_x\text{Se}_{1-x}$  provide intense light ranging from blue to violet, which may be tuned by varying the direct band gap by controlling the S concentration.<sup>1,2</sup> The electronic properties of CdS have attracted attention by its application in solar cells.<sup>3,4</sup> The design of such electronic devices is based on a detailed knowledge of the electronic band structure. In addition, the zinc-blende structure of ZnS and wurtzite structure of CdS are relatively simple and well characterized so that these materials are good candidates for theoretical model development in solid-state physics. Some theoretical calculations of ZnS (Refs. 5–18) and CdS (Refs. 10 and 16–25) have been reported. Some experimental results on the density of states, mostly determined from photoemission measurement, have been reported for CdS (Refs. 4 and 26–34) and ZnS.<sup>27,30,31,34,35</sup>

The electronic properties of IIB-VI compounds with IIB elements Zn, Cd, and Hg and VI elements S, Se, and Te are still not completely understood. It is now established experimentally that the  $d$  bands, derived from the IIB elements, lie in the subband gap between the lower valence band derived from the  $s$  orbital of the group-VI elements and the upper valence band derived from the  $p$  states of the group-VI elements and the  $s$  states of the IIB elements. The locations of these bands within the gap disagree with the best available calculations, however.

The problem may be traced to the difficulty of treating delocalized  $s$ - $p$  electrons and localized  $d$  electrons in the

same calculation. Older calculations, using orthogonalized-plane-wave (OPW) and Korringa-Kohn-Rostoker methods, are well adapted for treating  $s$ - $p$  bands, but usually ignored the  $d$  bands altogether, treating them as part of a frozen core. More current calculations use pseudopotential plane-wave and linearized augmented-plane-wave methods and the local-density approximation (LDA). These calculations, in common with most LDA calculations, underestimate the measured band gaps between valence-band and empty conduction-band states. They also locate the  $d$  bands higher in the subband gap than is observed in photoemission. The latest  $GW$  calculation on CdS has improved agreement with the measured band gap.<sup>19</sup> (The  $GW$  method includes the influence of self-energy and uses a self-energy operator that is a product of the Green's function  $G$  and the dynamically screened Coulomb interaction  $W$ .) However, the  $d$  location is still about 2 eV higher than experimental results. Some authors argue that this discrepancy between theory and experiment results from the fact that the photoemission process leaves a hole in the  $d$  bands that increases the binding of the  $d$  electrons. In any case, band gaps, subband gaps, bandwidths, and the precise locations of  $3d$  (ZnS) and  $4d$  (CdS) bands are important parameters for comparing experiment with theory, and no current calculations give good agreement with all of these parameters.

Some experimental data providing electronic density of states information are available for ZnS and CdS. Data are available from ultraviolet photoemission spectroscopy,<sup>30,31</sup> angle-resolved photoemission spectroscopy,<sup>4,29</sup> and x-ray photoemission spectroscopy (XPS).<sup>30,35</sup> In photoemission, the  $3d$  (Zn) and  $4d$  (Cd) electron spectra are very intense and dominate the weak  $s$  emission. This fact, in combination

with problems of sample charging, limits resolution for both the  $d$ -band and ( $s$ - $p$ )-band spectra and makes it difficult to precisely determine bandwidths and separations. Sample charging in insulators can result in variations in surface potential that modify the energy of emitted electrons, but not of photons. A few soft-x-ray absorption and emission results have been reported for ZnS and CdS.<sup>27,28</sup> Good-quality electron-beam-excited  $K$  and  $L$  emission spectra were reported for CdS, but an accurate interpretation of the spectra was not given.<sup>28</sup>

Recent publications show that the energy position of valence-band soft-x-ray fluorescence (SXF) spectra may shift and the relative magnitude of spectral features may change when spectra are excited by photons with energies near threshold.<sup>36-41</sup> All such effects may be attributed to an inelastic scattering process, usually called an electronic resonant Raman (ERR) process, in which energy is lost to an electronic excitation.<sup>42</sup> In different materials, the detailed nature of the electronic excitation is different. In crystalline Si, diamond, and graphite, changes in spectral shape and dispersion of spectral features with variation of the excitation energy are observed, which are attributed to  $k$  conservation between the photoelectron generated in the excitation process and the valence hole remaining after the coupled emission process.<sup>38,39</sup> In BN, the inelastic losses are coupled to a strong resonant elastic scattering process. Here the intermediate state of the scattering process is a localized core exciton and the final state a localized valence exciton state, so that the electronic excitation is strongly localized in real space.<sup>36,40,41</sup> In this paper, we report S  $L_{2,3}$  SXF spectra excited near threshold for both CdS and ZnS. Some weak modulation of spectral features in the upper valence band is observed immediately at threshold, which may be attributable to  $k$ -conserving transitions as in Si and C. However, for the present paper, the most significant result is that we are able to excite between the  $L_2$  and  $L_3$  thresholds so that a clean  $L_3$  spectrum is obtained for comparison with theory. The situation is very different for near-threshold excitation of the Zn  $M_{2,3}$  spectrum. Here a very strong and narrow inelastic peak dominates the fluorescence spectrum near threshold, providing a textbook example of an ERR process involving a localized electronic excitation of  $d$  electrons in a solid.

In this paper, we report our measurements on cubic ZnS and wurtzite CdS using SXF spectroscopy. The SXF spectra reported in this paper were made mostly at the U5 undulator beam line 8.0 of the Advanced Light Source (ALS) at Lawrence Berkeley National Laboratory. The electron-beam emission spectra, along with some early measurements with lower-resolution exciting light, were made on beam line U10A of the National Synchrotron Light Source (NSLS) at Brookhaven National Laboratory. In the remainder of this paper a brief description of experimental procedures is given in Sec. II. Results are reported in Sec. III and are discussed and compared with other work in Sec. IV.

## II. EXPERIMENTAL PROCEDURES

In soft-x-ray emission (SXE) spectroscopy, core electrons are excited by either energetic electrons or photons. The term ‘‘soft-x-ray fluorescence spectroscopy’’ is reserved for the

photon excited spectra. SXE spectra are produced when valence electrons make radiative transitions to empty core levels. Since the transitions are made to a localized core level of a particular atomic species and obey dipole selection rules, the spectra provide a measure of the local, angular momentum selected, partial density of states for one element of the material.

The SXF spectroscopy facility at the ALS consists of a 5-cm period undulator, a spherical grating beam-line monochromator, a sample chamber, and emission spectrometer. Light from the undulator is vertically focused onto the entrance slit of the monochromator; the monochromatized light is refocused horizontally onto the sample in the sample chamber. Incident light is measured by the photoemission current from a gold-coated screen placed immediately upstream of the sample. Soft x rays emitted from the sample are diffracted from a spherical ruled reflection grating and detected by a photon-counting area detector that is moved along a Rowland circle. During data acquisition, both the incident flux and the total emission flux imaged on the area detector are monitored.

The specifications of undulator beam line 8.0 at the ALS have been published.<sup>43</sup> Excitation fluxes available from the ALS undulator are about  $50\times$  greater than those available from our bending magnet beam line at the NSLS. Since the undulator is not a continuum source, both undulator and monochromator are scanned together to set the energy of the incident light. The extra intensity and improved monochromator available at the ALS makes it possible to excite spectra with higher resolution and reduced scattered light. At 163 eV, near the threshold for the S spectra, the full width at half maximum of the exciting beam was 0.4 eV at the ALS, compared with about 2.0 eV at the NSLS.

The emission spectrometer is an improved version of the spectrometer used at the NSLS, which has been described in detail elsewhere.<sup>44-46</sup> The detector is scanned using a computer controlled XY plus rotation table, which permits the instrument to be scanned along either a 5.0-m or 10.0-m Rowland Circle. The instrument is fitted with four gratings that, together with the two Rowland circle diameters, permit the instrument to measure spectra with energies from about 50 to 1200 eV with good resolution. A 5-m, 1200-l/mm grating was used to record the S  $L$  spectra reported here and a 5-m, 600-l/mm grating to record the Zn  $M$  spectra. The beam line produces horizontally polarized x rays and the spectrometer measures light dispersed in the horizontal plane, so that it measures emission in the  $p$ -polarization rather than  $s$ -polarization direction. Further specifications for the ALS emission spectrometer have been published elsewhere.<sup>43</sup>

The area detector is a commercial Quantar detector and consists of a stack of 40-mm-diam microchannel plates, which provide a localized current pulse to a four-cornered resistive sheet detector, with an active linear region of  $25\times 25$  mm<sup>2</sup>.<sup>46</sup> XY position information is derived from the fraction of the pulse that arrives at each corner. The resolution of the detector is about 50  $\mu$ m. The full resolution of the detector is used in the dispersion direction. In the transverse direction, pixels are binned so that the spectrum is divided into 16 slices, which may be horizontally translated to remove curvature in the spectrum due to aberrations. For both the S  $L$  and the Zn  $M$  spectra, the detector records a spectral

region approximately 20 eV wide. For wider spectra, sections are recorded by moving the detector along the Rowland circle at about 10-eV intervals and splicing the acquired spectra together. Extensive calibration procedures are used to correct for variations in sensitivity of the detector system across the detector face. The great virtue of this detector system is that it is a true photon-counting detection system with excellent discrimination against low level noise from the microchannel plates, so that signal to noise is usually determined only by the statistical noise of the signal pulses.

The electron-beam spectra reported here were measured at our NSLS beam line using an emission spectrometer having very similar resolution to the ALS spectrometer. Photon-excited spectra were also recorded at the NSLS, but because of the poorer resolution available there for exciting the spectra, the SXF spectra reported here are mostly those recorded at the ALS. 3000-eV electrons and beam currents of  $\leq 0.3$  mA were used for electron-beam excitation. Sulfur  $L$  spectra were also excited with 1000- and 1500-eV electrons to check for self-absorption effects, but were found to produce very similar spectra.

The CdS sample is a bulk crystal with wurtzite structure grown by molecular-beam epitaxy. Cubic ZnS thin-film samples with (001) and (111) orientations and thicknesses of 5200 and 2100 Å and the  $\text{ZnS}_{0.5}\text{Se}_{0.5}$  sample were provided by Oak Ridge National Laboratory.<sup>47</sup> Immediately before mounting in the sample chamber, all samples were etched in dilute  $\text{H}_2\text{SO}_4/\text{H}_2\text{O}$  to remove oxide layers.

During measurements with electron-beam excitation, pressures were  $\leq 5 \times 10^{-9}$  Torr and with photon excitation,  $\leq 1 \times 10^{-9}$  Torr. The excitation region with electron-beam excitation was a spot of  $\leq 0.2$  mm diameter and with photon excitation a rectangle with dimensions of approximately  $0.2 \times 1.0$  mm<sup>2</sup> aligned along the input slit of the emission spectrometer. Visible luminescence from the samples greatly simplified proper alignment of the electron or photon excitation beam.

Several different experiments were performed. Using 3-keV electron-beam excitation, the S  $L_{2,3}$  and the Zn  $M_{2,3}$  spectra of CdS, ZnS,  $\text{ZnS}_{0.5}\text{Se}_{0.5}$  and ZnSe were measured. The sulfur spectra were also measured with 174-eV photon excitation, an energy well above the sulfur  $L_{2,3}$  threshold, in order to compare spectra excited by electrons and photons. Finally, for ZnS and CdS, spectra were excited for a range of energies near threshold in order to look for modifications of the spectra with near-threshold excitation.

For the threshold studies, spectra are normalized to the total number of incident photons taken to be equal to the incident x-ray flux ( $I_0$ ) times the exposure time ( $\Delta t$ ). We also obtain some data on the absorption near threshold by plotting the partial fluorescent yield determined as  $Y(E) \propto (\text{spectral area}) / (I_0 \Delta t)$ , as a function of photon energy  $E$ .  $I_0$  was taken as proportional to the current from the photoemission flux monitor located in the incident light path of the ALS. The spectral area can be selected as a part of the valence band or as the entire recorded spectrum. It should be noted that this fluorescence yield does not provide an accurate measure of the total absorption. Light is absorbed above an x-ray edge and emission occurs below it so that the emission depth is generally much greater than the absorption depth, causing the yield to saturate at a nearly constant value

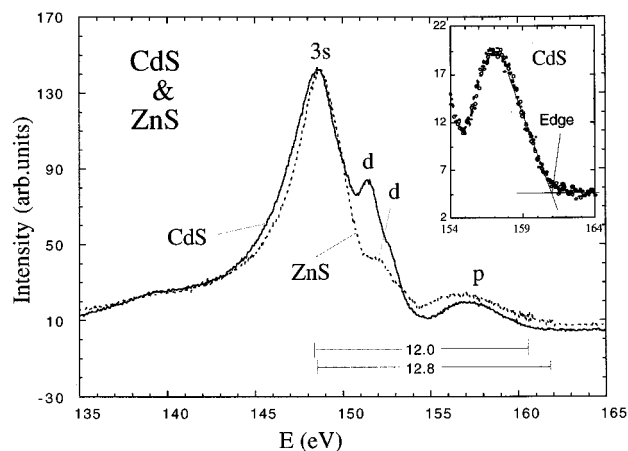


FIG. 1. S  $L_{2,3}$  soft-x-ray spectra of CdS and ZnS with 3-keV electron-beam excitation. The solid line is for CdS and the dashed line is for ZnS. The inset shows the CdS spectrum at the valence-band maximum.

rather than to decrease as expected above the absorption edge. However, the fluorescence yield provides a measure of the onset of absorption and permits the determination of the band gaps. They are also frequently useful for identifying new radiative emission channels when studying inelastic-scattering phenomena near threshold.

### III. RESULTS

#### A. Sulfur $L_{2,3}$ spectra of CdS and ZnS

We first present data obtained for the sulfur  $L_{2,3}$  spectra. Figure 1 depicts these spectra for ZnS and CdS with 3-keV electron-beam excitation at NSLS. The spectra of CdS and ZnS are very similar, but with some difference in detail. Three spectral features are present that can be identified with large-scale valence-band features. The largest peaks at the lowest-energy position, which peak at 148.7 eV for ZnS and 148.6 eV for CdS, are derived from the sulfur  $3s$  orbital and are referred to as the lower valence band (LVB). Measurements on a variety of transition metal-sulfur compounds also show a strong peak at nearly the same energy position.<sup>48</sup> A broad, weak peak centered at about 156 eV for ZnS and 157 eV for CdS is located at the position of the upper valence band (UVB) derived from the hybridization of S  $3p$  and Cd(Zn)  $s$  and  $p$  orbitals. Its presence in the spectra is evidence of the covalent bonding that contributes to the stabilization of the tetrahedral coordinated wurtzite and zincblende structures.

The narrow peaks located at 151.4 eV in CdS and at 152.1 eV in ZnS are interesting features. These peaks are derived from the Zn  $3d$  and Cd  $4d$  orbitals that overlap onto the sulfur site. Theoretical calculations agree that in these compounds, the  $d$  states form a narrow band lying in a valence-band subband gap associated with the ionic potential of these II-VI compounds.<sup>8,11</sup> The location of this  $d$  band as lying in the gap between the two valence bands has also been confirmed from photoemission measurements for ZnS, CdS, and HgS.<sup>34</sup> A low-energy satellite is observed about 9 eV below the LVB. It probably results from a ‘‘shakeup’’ process in which a valence-band to conduction-band electronic transition reduces the energy of the radiated photon.<sup>37</sup>

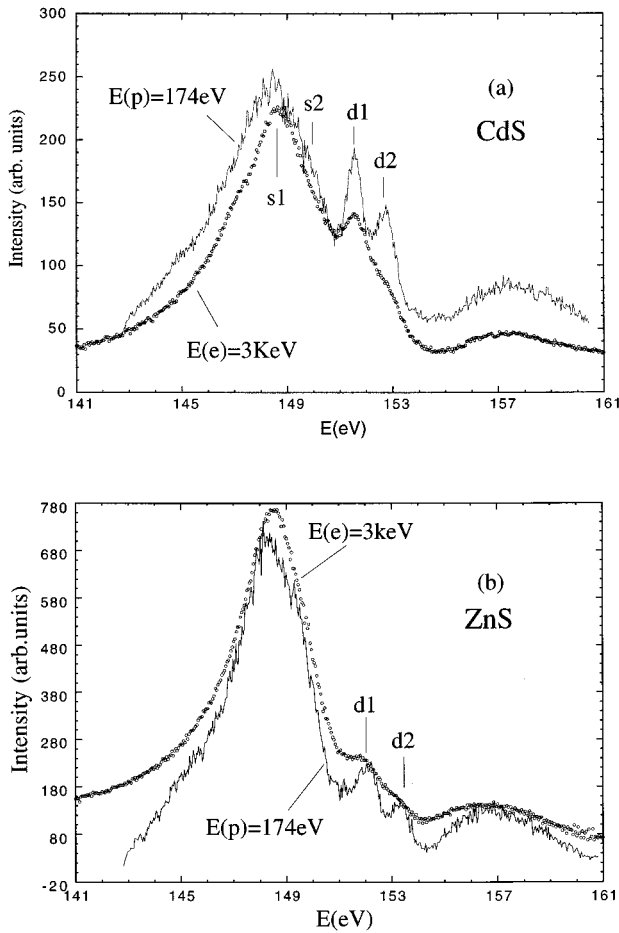


FIG. 2. Comparison of S  $L_{2,3}$  spectra for 3-keV electron-beam and 174-eV photon excitation: (a) CdS and (b) ZnS.

The upper edge of the valence band [valence-band maximum (VBM)] is determined as shown in the inset of Fig. 1 from the crossing point of the extrapolated spectral edge and the base line. This value of the VBM is properly associated with the  $L_2$  edge, which lies above the  $L_3$  edge by the value of the spin-orbit splitting of the sulfur  $2p$  core levels. A correction for this splitting must be made before comparisons with theoretical densities of states are made.

Figures 2(a) and 2(b) exhibit sulfur  $L_{2,3}$  spectra from CdS and ZnS excited by electrons (dots) and photons at the ALS (solid line). The most notable feature is that the photon excited spectra are greatly sharpened with respect to the electron-beam spectra. In the photon-excited spectra, the doubling of Cd(Zn)  $d$  bands due to the spin-orbit split core levels are clearly resolved. The sulfur  $s$  band is also significantly broadened by the overlapping  $L_2$  and  $L_3$  spectra. We present below (Figs. 3, 4, 6, and 8) spectra in which the  $L_2$  spectra are suppressed. Both the 1:2 intensity ratio of spin-orbit split  $d$  bands and their separation of about 1.1 eV are consistent with the spin-orbit splitting of sulfur  $2p$  core level. The observed spectra can be interpreted in a straightforward manner as the superposition of an  $L_3$  spectrum and an  $L_2$  spectrum of half the intensity displaced to higher energy by 1.15 eV. The energy positions of various features of these CdS and ZnS sulfur  $L$  spectra taken from electron-beam excitation at NSLS are summarized in Table I.

TABLE I. Energy positions of major features in the S  $L_{2,3}$  spectra of ZnS and CdS from 3-keV electron-beam excitation, all in units of eV. EB, electron-beam excitation; LVB, lower valence band; UVB, upper valence band; VBM, valence-band maximum.

Compound	$L_{2,3}$ (EB)	Refs. 30 and 34 (EB)	Ref. 28
ZnS			
LVB peak	148.7	148.4	
$d1$	152.1	152.0	
$d2$	153.2	153.1	
UVB peaks	156.5	157.8	
VBM	161.5	161.5	
CdS			
LVB peak	148.6	148.4	148.1
$d1$	151.4	151.0	151.1
$d2$	152.6	152.2	152.2
UVB peak	157	156.7	156.4
VBM	161.5	162	

The  $L_3$  spectra can be obtained from a deconvolution of  $L_{2,3}$  spectra using an  $L_2/L_3$  intensity ratio of 1/2 and a spin-orbit splitting of 1.15 eV. It is more accurate, however, to use the improved intensity and resolution of the ALS beam line to tune between the  $L_2$  and  $L_3$  thresholds in order to excite the  $L_3$  spectrum alone. Spectra obtained in this way are shown for CdS in Fig. 3 and ZnS in Fig. 4. Other spectra excited near threshold are presented in Sec. III C. These spectra are divided by  $E^3$  to remove extra frequency factors that appear in the optical transition matrix elements, in order to make them more directly comparable with calculated densities of states.

The  $L_3$  spectra show several important features that are obscured in the  $L_{2,3}$  spectra. Both the upper (UT) and lower edges (UB) of the UVB and its broad structural features are resolved. The peak of the LVB and identifiable features of the  $d$  bands ( $d1$  and  $d3$ ) and UVB ( $U1$ ,  $U2$ , and one more  $U3$  in ZnS) are identified and their energy positions tabulated in Table II. Two  $d$ -band features are well separated in CdS and partially resolved in ZnS. Their relative ratio is about 0.4 for both materials. The weaker, low-energy feature of the  $d$  bands in both materials was not observable in the

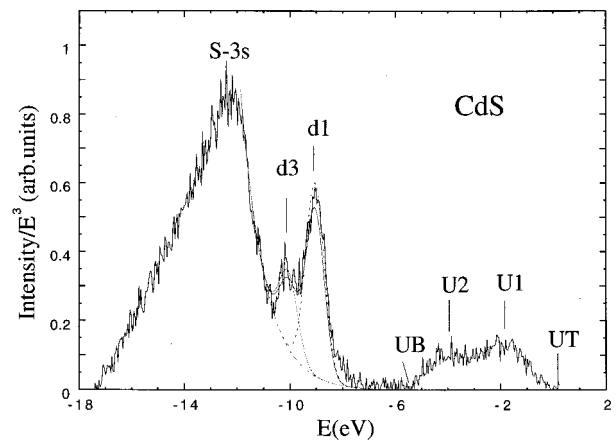


FIG. 3. S  $L_3$  spectrum of CdS with excitation between the  $L_2$  and  $L_3$  thresholds.

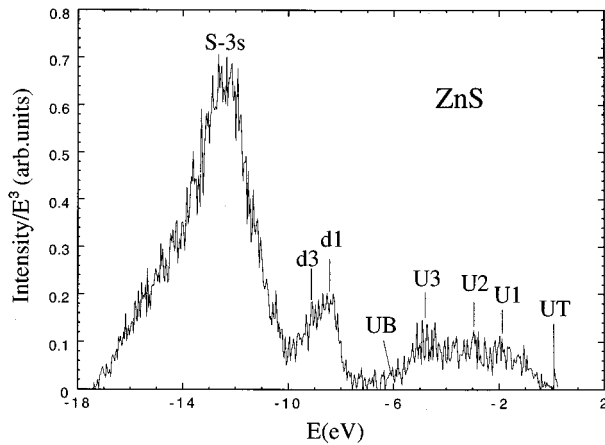


FIG. 4. S  $L_3$  spectrum of ZnS with excitation between the  $L_2$  and  $L_3$  thresholds.

$L_{2,3}$  spectrum and was revealed only by the suppression of the LVB of the  $L_2$  spectrum. These results from the  $L_3$  spectra of CdS and ZnS are listed in Table II along calculated values of the identified spectral features. The remarkable improvement in resolution observed with photon excitation as compared with electron excitation is discussed further in Sec. IV.

#### B. Zinc $M_{2,3}$ spectra of ZnS and $\text{ZnS}_{0.5}\text{Se}_{0.5}$

In Fig. 5(a) we display zinc  $M_{2,3}$  electron-excited spectra for ZnS and  $\text{ZnS}_{0.5}\text{Se}_{0.5}$  taken with electron-beam excitation at NSLS. The spectra are normalized to the peak at 74.1 eV. This strong band peaking at 74.1 eV, which decreases in relative magnitude with decreasing S concentration, is the second-order sulfur  $L_{2,3}$  spectrum. The wider features centered at 78.5 and 81.2 eV, which have a separation of 2.7 eV and the intensity ratio of 2:1, are double  $d$  bands from the zinc  $3p$  core-level spin-orbit splitting. The peaks correspond to transitions from the  $d$  bands to the  $3p_{3/2}$  ( $M_3$  spectrum) and  $3p_{1/2}$  ( $M_2$  spectrum) core levels, respectively. The structure extending to about 90 eV is derived from the upper

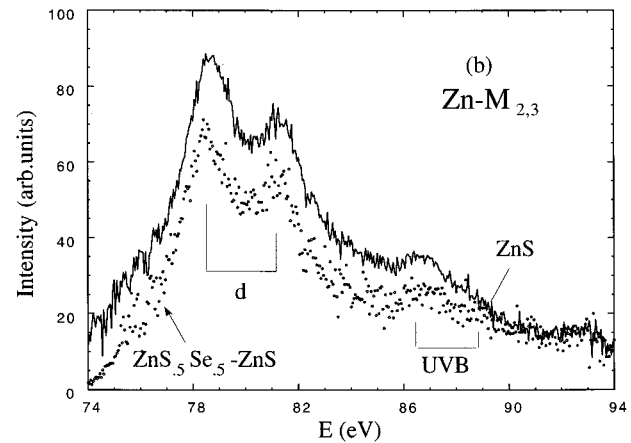
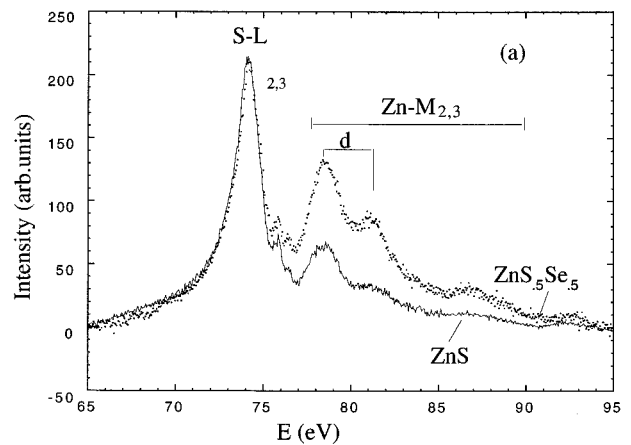


FIG. 5. Zn  $M_{2,3}$  spectra of ZnS and  $\text{ZnS}_{0.5}\text{Se}_{0.5}$  with 3-keV electron-beam excitation: (a) combined Zn  $M_{2,3}$  and second-order S  $L_{2,3}$  spectra and (b) reduced Zn  $M_{2,3}$  spectra.

valence band. The peak at 93 eV is probably a third-order carbon  $K$  spectrum associated with carbon contamination of the sample.

In Fig. 5(b), two methods have been used to obtain the zinc  $M_{2,3}$  spectra. In one, the first-order S  $L_{2,3}$  spectrum is

TABLE II. Energy positions of principal features in the S  $L_3$  spectra of CdS and ZnS, all in units of eV. UT, upper edge of the UVB; UB, lower edge of the UVB; U1,U2,U3, peaks in the valence band; Calc., theory; Expt., our data.

Spectral feature	CdS (Expt.)	CdS (Calc.) <sup>a</sup>	ZnS (Expt.)	ZnS (Calc.) <sup>b</sup>
UT	0.0	0.0	0.0	0.0
U1	-1.8	-1.1	-1.9	-2.0
U2	-3.8	-4.3	-3.0	-4.5
U3			-4.7	
UB	5.4		6.0	
$d_1$	-9.0	-7.8	-8.4	
$d_3$	-10.1	-7.6, -7.16	-9.1	
$\Delta E(d_1 - d_2)$	1.05	<0.6	0.6	
Ratio ( $d_1/d_2$ )	0.40		0.41	
$\Delta E$ ( $2p$ spin splitting) <sup>c</sup>	1.15	1.18	1.18	
S $3s$	-12.2	-11.6	-12.4	-12.0

<sup>a</sup>Reference 20.

<sup>b</sup>Reference 16.

<sup>c</sup>From  $L_{2,3}$  spectra.

TABLE III. Energy positions of the spectral feature in Zn  $M_{2,3}$  spectra of ZnS, all in units of eV. EB, data from ZnS<sub>0.5</sub>Se<sub>0.5</sub> with electron-beam excitation; 127 eV, data from photon excitation with an energy of 127 eV.

	$M_{2,3}$ (alloy, EB)	$M_{2,3}$ (127 eV, ZnS)
$d1$	78.5	78.5
$d2$	81.2	81.3
peaks at UVB	86.6,88.9	
VBM	89.9	

halved in energy, normalized to the peak at 74.1 eV, and subtracted from the ZnS spectrum in Fig. 5(a). In the other, the ZnS spectrum in Fig. 5(a) was subtracted from the ZnS<sub>0.5</sub>Se<sub>0.5</sub> spectrum. In both cases, the broad  $M_2$  and  $M_3$  spectra are resolved. Compared with  $d$  bands visible as overlap spectra in the sulfur  $L_{2,3}$  spectra, these bands are much broader. The main contribution to this extra broadening is the  $M_{2,3}$  core-level lifetime broadening of about 2.0 eV.<sup>49</sup> The energy position of band features derived from the zinc  $M$  spectra are presented in Table III. Using the same method described in Fig. 1, we estimate the  $d$ -band separation from the VBM to be 8.7 eV from these spectra. Values derived from the sulfur  $L_3$  spectra are 8.4 eV with photon excitation and 8.3 eV with electron-beam excitation after subtraction of the spin-orbit splitting. The larger  $d$  band to VBM value obtained from the zinc  $M$  spectra may be attributed to the large lifetime broadening ( $\approx 2$  eV) of the Zn  $3p$  core levels, which produces an apparent shift of the VBM to higher energies. The lifetime broadening of the S  $L_{2,3}$  is nearly two orders of magnitude smaller. We consider the value of 8.4 eV obtained from the selectively excited S  $L_3$  spectrum to provide the best measurement of the positioning of the  $d$  band with respect to the VBM in ZnS. The comparable  $d$  band to VBM separation in CdS is 9.0 eV.

### C. Threshold effects in CdS and ZnS

The emission spectra of ZnS and CdS were measured near threshold with photon excitation at NSLS and remeasured at ALS to gain better resolution. Figure 6 presents the results obtained for ZnS and Fig. 8 for CdS.

Figure 6(a) taken with an excitation bandwidth of approximately 2 eV at NSLS, are typical of SXF spectra obtained at that facility. These spectra are normalized to the integrated excitation flux determined by multiplying the beam current by excitation time. Two separate groups of spectra are seen clearly. The narrow high-energy peaks are produced by elastically scattered light from the incident beam. The lower-energy spectra, which remain fixed in energy, are the fluorescence spectra. In Fig. 6(b), spectra taken near threshold with higher resolution at the ALS are presented. In Fig. 7, using the data of Fig. 6(a), the energy shift of the peak of the LVB near threshold and the intensity variation of various features of the fluorescence spectra are plotted as a function of incident energy. The curve marked with VB is a plot of the integrated intensity of the emission spectrum as a function of the excitation energy and thus provides a plot of fluorescence yield of ZnS near threshold. The fluorescence of CdS obtained with near-threshold excitation

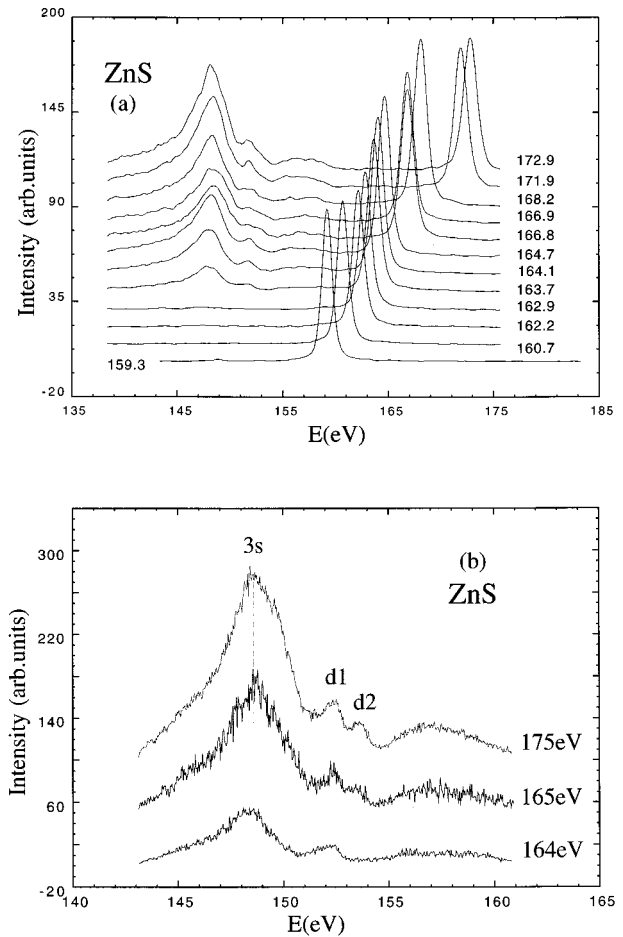


FIG. 6. S  $L_{2,3}$  spectra of ZnS with the photon excitation near threshold. (a) NSLS data obtained with the 2-eV excitation bandwidth. (b) ALS data obtained with the 0.4-eV excitation bandwidth showing suppression of the  $L_2$  spectrum.

at the ALS are presented in Fig. 8(a). Figure 8(b) is a fluorescence yield curve of CdS measured at ALS by electronically integrating the total fluorescence yield between 145 and 160 eV as the incident energy is scanned and thus is a higher-resolution version of absorption curve presented for

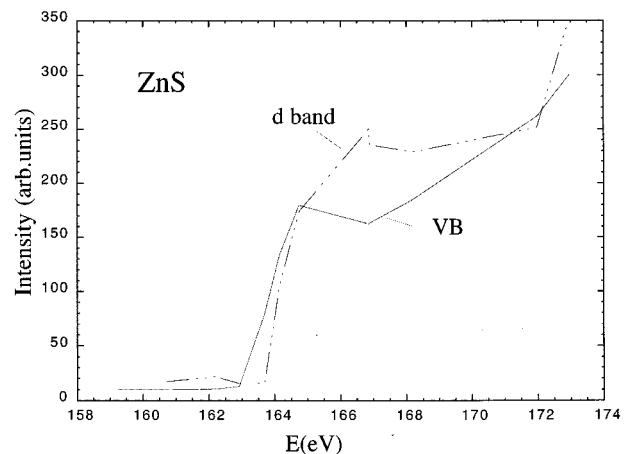


FIG. 7. Fluorescent yield of ZnS derived from Fig. 6(a). The solid line is the yield from the whole valence band and the dashed line is the yield from the  $d$  bands.

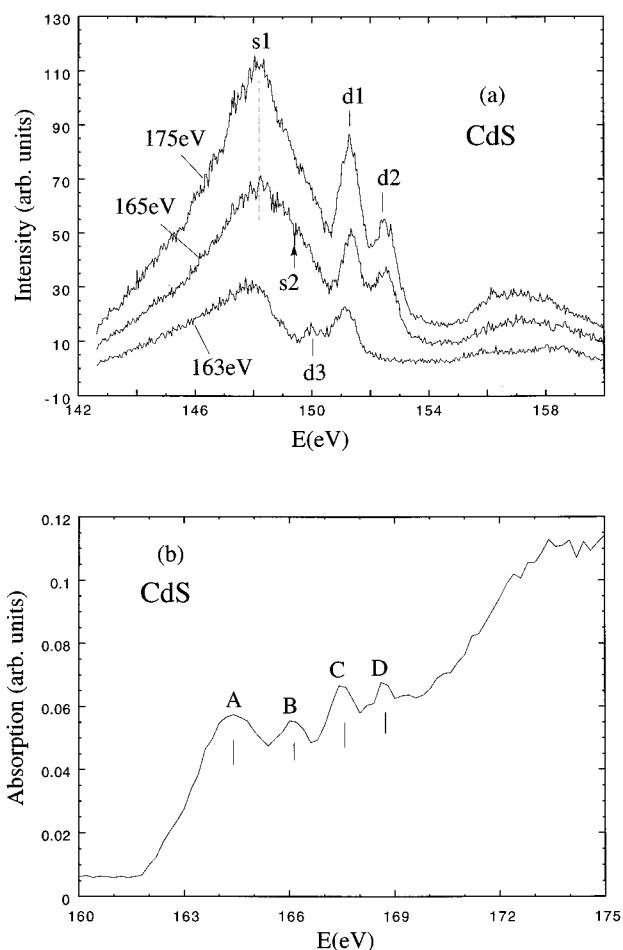


FIG. 8. S  $L_{2,3}$  spectra of CdS with the photon excitation near threshold. (a) Emission spectra of CdS taken with the 0.4-eV excitation bandwidth showing suppression of the  $L_2$  spectrum. (b) Fluorescent yield of CdS.

ZnS in Fig. 7. These absorption curves determine the core-level to conduction-band spacing and when combined with emission spectra may be used for the determination of band gaps.

It is also possible to obtain a measure of the position of the absorption threshold by monitoring the sample current produced by photoemission as a function of excitation energy. The photoemission current increases at threshold due to the opening of new Auger deexcitation channels. Thresholds derived from such measurements are in good agreement with those derived from the x-ray yields. Two papers reported absorption experiments at the sulfur  $L_{2,3}$  edge for cubic ZnS (Ref. 27) and CdS.<sup>27,28</sup> The onset of absorption and the lowest absorption peak that we observe at about 164 eV are consistent with these published results.

Two principal qualitative modifications are observed for near-threshold excitation of spectra. Separate thresholds are visible for the  $L_3$  and  $L_2$  spectra. The higher-energy  $L_2$  spectrum is only observed with excitation above about 165 eV for ZnS and CdS. The second qualitative feature is that for excitation within about 2 eV of its threshold, there is an enhancement of the  $L_2$  spectrum relative to the  $L_3$  spectrum. More striking modifications of spectra sometimes observed in other materials with near-threshold excitation are not ob-

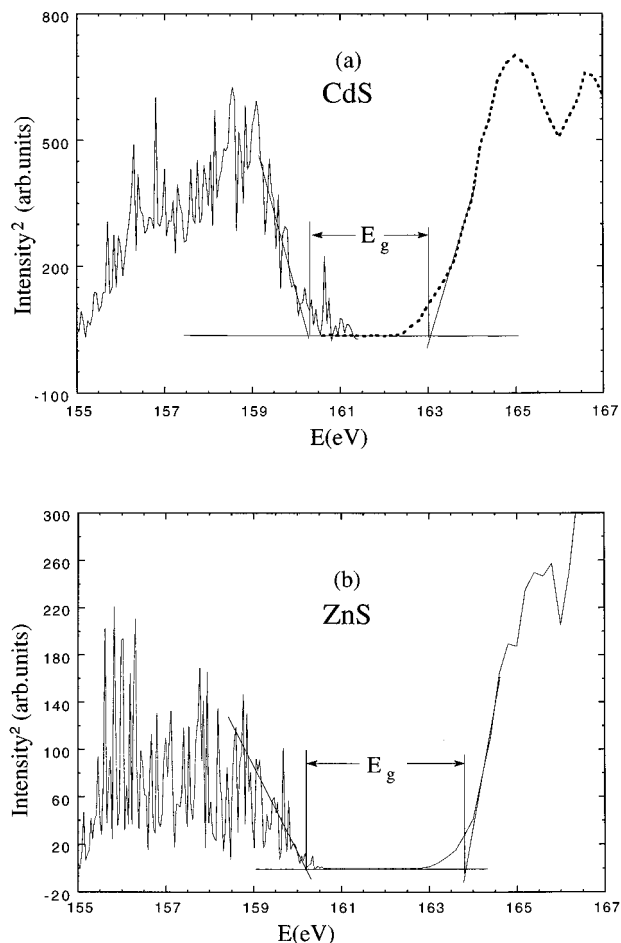


FIG. 9. Conduction- and valence-band edges and band gaps: (a) CdS and (b) ZnS.

served for the S  $L$  spectra of these materials. As will be shown below, strong electronic resonance Raman effects are observed for the Zn  $M$  spectra.

A measure of the energy band gap is provided by the energy difference between the top edge of the UVB measured in the emission spectra and the bottom of the conduction band determined from the absorption spectrum. Near a band edge, the density of states will vary as  $(E - E_0)^{1/2}$ . In order to determine the top of the valence band and the bottom of the conduction band, we plot the square of the spectral intensity versus energy. The band gaps are determined by extrapolating straight lines fitted to the spectra to the baseline. To eliminate the influence of spin splitting on the band-gap determinations, SXF spectra excited with photons between the  $L_3$  and  $L_2$  edges were used to determine the band gaps. Figure 9 shows the band gaps determined in this way for ZnS and CdS. The band gaps were determined in this way to be 2.7 eV for CdS and 3.6 eV for ZnS using ALS data and 2.6 eV for CdS and 3.6 eV for ZnS using NSLS data.

#### D. Inelastic scattering near threshold in the Zn $M_{2,3}$ spectrum of $\text{ZnS}_{0.5}\text{Se}_{0.5}$

Zn  $M_{2,3}$  spectra of ZnS and  $\text{ZnS}_{0.5}\text{Se}_{0.5}$  spectra excited near threshold show strong inelastic scattering effects that

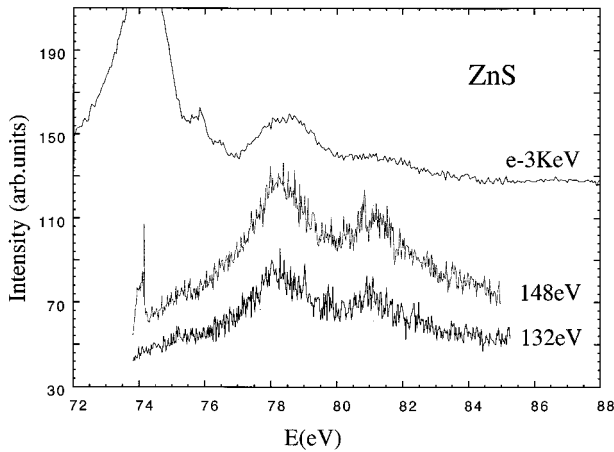


FIG. 10. Zn  $M_{2,3}$  spectra of ZnS with electron-beam and photon excitation.

can be explained using a simple model and an inelastic scattering theory based on second-order perturbation theory. As noted previously, this scattering is often called electronic resonance Raman scattering.

For the sulfur  $L_{2,3}$  spectra, which were the principal focus of the previous sections, the use of photon excitation near threshold had value for sharpening the observed spectra and for separating the  $L_2$  and  $L_3$  spectra, but there is little evidence of the contribution of the one-step inelastic scattering processes that have been observed near threshold in many other materials. Consequently, our analysis was devoted primarily to a discussion of the traditional density of states information that can be obtained from SXE spectroscopy.

The case is very different for the near-threshold excitation of the Zn  $M_{2,3}$  spectra of ZnS and  $\text{ZnS}_{0.5}\text{Se}_{0.5}$ , which show dramatic inelastic scattering effects, whose principal features can be understood with the inelastic scattering theory developed by Tulkki and Åberg.<sup>42</sup> The data presented here are for the most part taken with the  $\text{ZnS}_{0.5}\text{Se}_{0.5}$  sample, for which the most complete data set is available, but essentially the same features are observed for Zn spectra ZnS.

In Fig. 10 a photon-excited Zn  $M_{2,3}$  spectrum of ZnS is plotted along with the electron-beam-excited spectrum presented previously in Fig. 5. The spectra excited with 132- and 148-eV photons are excited well above threshold have the properties of ordinary SXE spectra and are dominated by the strongly broadened transitions from the Zn  $3d$  levels in the valence bands to the spin-orbit split Zn  $3p$  core levels.

The effects of inelastic scattering are dramatically illustrated by the Zn  $M$  spectra of  $\text{ZnS}_{0.5}\text{Se}_{0.5}$  presented in Fig. 11. In this figure, the elastic and inelastic peaks are shown on the same energy scale for near-threshold excitation between 89 and 98 eV and for an energy of 148 eV well above threshold. The 148-eV spectrum is similar to those presented above for ZnS and is a normal fluorescence spectrum, in which the excitation and deexcitation processes are decoupled. The narrow peak at 74 eV is the second order of the elastically scattered incident beam.

The fluorescence spectra excited at photon energies between 89 and about 96 eV, however, show dramatic evidence of the one-step inelastic-scattering process. As the photon

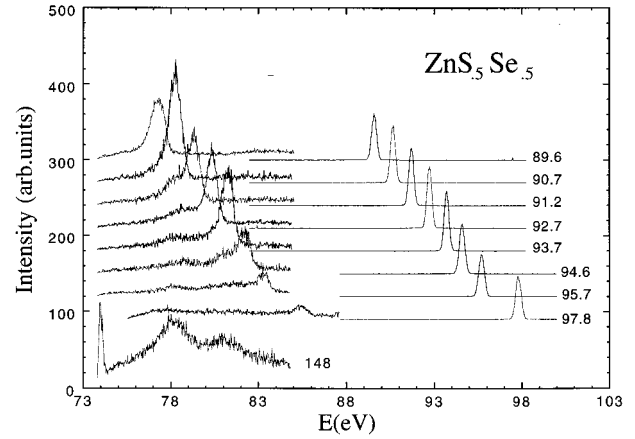


FIG. 11. Zn  $M_{2,3}$  spectra of  $\text{ZnS}_{0.5}\text{Se}_{0.5}$  excited near threshold.

energy is increased within this range, a strong inelastic scattering less than 2 eV wide moves through the normal fluorescence spectrum. Several features of this peak are noteworthy. First, within experimental resolutions and accuracy, it exactly tracks the elastic peak at about 12.4 eV lower energy, as is evident from Table IV, which lists the positions of the peaks taken from the experimental spectra. Second, the peak is much narrower than the normal fluorescence spectrum; its overall width of less than 2 eV is comparable to that observed for the  $d$ -band peak in the sulfur  $L_3$  spectrum. Third, its relative intensity as it moves through the normal fluorescence spectrum is approximately proportional to the intensity of the ordinary fluorescence spectrum, reaching maxima at energies of about 78 and 81 eV, the peaks of the normal fluorescence spectra. All of these features may be readily understood using the ERR formalism discussed further below.

#### IV. DISCUSSION

Our results are consistent with previous measurements providing density-of-states information for CdS and ZnS. A comparison may be made with previously reported electron-beam-excited sulfur  $K$  and  $L_{2,3}$  spectra of CdS.<sup>27,28</sup> These measured  $L$  spectra are in good agreement with our results,

TABLE IV. Observed inelastic energy losses in x-ray scattering near the Zn  $M_{2,3}$  edge.

$E$ (Elastic)	$E$ (Inelastic)	$D\Delta E$ (center-center)
89.5	77.2	12.3
90.7	78.3	12.4
91.7	79.3	12.4
92.7	80.3	12.4
93.7	81.2	12.5
94.6	82.2	12.4
95.6	83.3	12.4
97.8	85.4	12.4
Average 12.4		

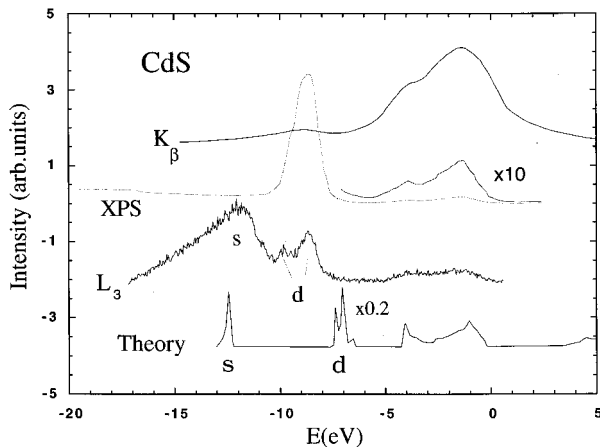


FIG. 12. Comparison of experimental and theoretical results for CdS.

except for minor differences in the absolute energies assigned to spectral features, which result from different spectrometer calibrations. The  $L_3$  and  $K$  spectra can be compared by aligning the spectra at the valence-band maximum as shown in Fig. 12. The major peak in the  $K$  spectrum, which provides a measure of the  $p$  partial density of states, overlaps the weak upper valence band identified in our data, but no structure is present at the position of the lower valence band. A similar comparison can also be made with XPS data for both ZnS and CdS.<sup>30</sup> These spectra are dominated by the Zn 3d and Cd 4d spectra, but also clearly resolve the upper valence band. The XPS spectrum of CdS and a calculated spectrum are also plotted in Fig. 12.

In Tables I and II, the locations of spectral features observed with various spectroscopies are compared. Energies are referenced to the valence-band maximum, which is difficult to ascertain exactly, so that the accuracy of listed values is limited to about 0.1 eV. Differences in spectral features, such as the determination of the spin-orbit splitting of the sulfur  $p$  levels, may be determined with greater accuracy.

The results from all measurements are consistent with the general picture that the lower valence band is  $s$ -like and derived almost entirely from the sulfur 3s orbital. The upper valence band is derived primarily from the Cd(Zn)  $s$  and  $d$  states and the sulfur 3p states with the small admixture of sulfur  $s$  states that is characteristic of materials with partially covalent bonding. The Zn(Cd)  $d$  states, which dominate the XPS spectrum in Fig. 12 and the Zn  $M_{2,3}$  spectra of Fig. 5, appear in the sulfur  $K$  spectra as weak crossover transitions. To facilitate comparisons with theory, experimental energy separations of spectral features derived from the various spectroscopies are compared in Tables I and II. These include measures of the spin-orbit splitting of the sulfur  $L$  core levels, the energy separations between the valence-band maximum, and peaks identified in the upper and lower valence bands and the Zn(Cd)  $d$  bands, and energy separations between  $d$ -band and valence-band features. These energy separations were taken from the  $L_3$  spectrum of Figs. 3 and 4, except that spin-orbit splitting of  $d$ -band energies is taken from the  $L_{2,3}$  spectra.

In Table II, the energy separations are also compared with theoretical calculations. The agreement is generally satisfactory, with the exception that calculations systematically

place the  $d$  bands too close to the upper valence band and the measured valence- to conduction-band gap is larger with all experimental spectroscopies than indicated by LDA calculations. The best agreement is found with the GW (Ref. 19) and modified OPW (MOPW) calculations, which include effects of exchange and correlation.<sup>10,11</sup> The widths of the  $d$  bands and their positions with respect to the UVB are in good agreement with the photoemission data. The  $d$  bands in  $L_3$  spectra are about 2 eV wide and clearly show two components ( $d1$  and  $d3$ ) in Figs. 3 and 4. This doublet is also observed in the photonemission data and was attributed by Ley *et al.*<sup>30</sup> to the combined effect of spin-orbit interaction and crystal-field interactions. The only calculation that includes the  $d$  band gives a width of about 1 eV.<sup>13</sup> The photoemission results indicate a  $d$  splitting of about 0.8 eV for CdS compared with our value of 1.1 eV. In ZnS, we observed an extra shoulder, indicating the presence of a barely resolved peak  $d3$  split by 0.5 eV from  $d1$ .

Important features of the spectra are the narrow overlap peaks from the Cd and Zn  $d$  bands. The magnitude of these peaks in the sulfur  $L$  spectra provide a measure of the overlap of the  $d$  states onto the sulfur 2p cores. An experimental measure of the relative overlap is provided by the relative magnitude of these peaks normalized to the sulfur 3s peak at 148 eV. Normalization to the sulfur 3s peak compensates for most of the experimental factors affecting this comparison. The experimental value of this ratio is  $I(\text{Zn } 3d)/I(\text{Cd } 4d) = 0.36$ .

The decay of a core hole in a single x-ray-emission channel is given by

$$W_{fi} \propto E^3 |\langle \phi_f | t | \phi_i \rangle|^2,$$

where  $E$  is the energy of emitted x ray,  $t$  is the dipole operator, and  $\phi_f$  and  $\phi_i$  are the final- and initial-state wave functions.<sup>50</sup> Assuming that the dipole matrix elements are approximately equal for these two very similar systems, we obtained a calculated estimate of this ratio by calculating the two-center overlap integral between the Cd(Zn) 4d(3d) orbital and the sulfur 2p states calculated using atomic orbitals<sup>51</sup> and the Cd(Zn)  $S$  spacing of the two materials.<sup>52</sup> This calculation yields a ratio of 0.74 or nearly twice the experimental value. The large difference between the experimental value and the theoretical result suggests that a more thorough theoretical treatment would be of interest.

In Figs. 2(a) and 2(b), it is obvious that the  $d$ -band overlap peaks and other spectral features in photon excited spectra are sharper than those excited by an energetic electron beam. This sharpening of the spectra is most prominent for the  $d$ -band overlap peaks, but is also present for the sulfur 3s peak. This sharpening is *not* typical of the  $L$  spectra we have observed in other light elements and light element compounds, where no difference is usually seen between electron-beam-excited spectra and spectra excited by photons at energies well above threshold. Such broadening is observed, however, in the  $L$  spectra of transition metals such as Fe and Cu and is attributed to excitation of spectator holes in the  $d$  bands of these metals and their compounds.<sup>53</sup> We believe that spectator holes in the Cd and Zn  $d$  bands may be responsible for the excess broadening observed in the electron-excited spectra. More generally, charge trapping on

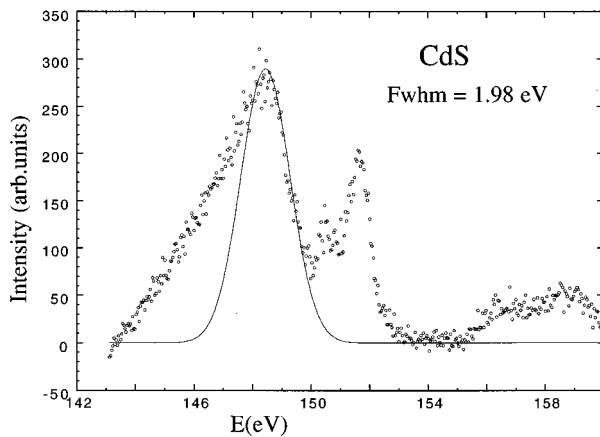


FIG. 13. Gaussian fit to the  $S\ 3s$  band of the  $S\ L_3$  spectrum of CdS to determine the valence hole lifetime.

neighboring atoms resulting from a variety of mechanisms associated with intense electron bombardment might contribute to the broadening of these levels.

The weak low-energy satellite centered at 139 eV is interpreted as an inelastic shakeup deexcitation process in which the energy of the emitted x ray is reduced by the energy required to excite one electron from the valence to conduction bands. These weak inelastic peaks have been observed in many systems and have been carefully studied by Livins and Schnatterly for Si.<sup>54</sup>

An important source of broadening in emission spectra is the lifetime broadening of the valence hole that remains after radiative recombination. Near the VBM in materials with a band gap, only electron-phonon scattering affects the valence-hole lifetime so that core-hole broadening is the factor limiting spectral resolution. For energies more than about two gap widths below the VBM, electron-electron scattering provides the major broadening mechanism for the observed spectra. It is possible to obtain an estimate of this electron-electron scattering lifetime by measuring the width of features in the emission spectra. We have obtained an estimate of this broadening by fitting a Gaussian function to the upper edge of the  $S\ 3s$  peak in Fig. 13. A fit to the lower edge of the peak is not useful due to the presence of the inelastically scattered electrons described in the preceding paragraph. The instrumental broadening in this range is small (0.15 eV). The full width at half maximum (FWHM) widths attributable to lifetime broadening are about 2.0 and 2.2 eV, respectively, for CdS and ZnS. This translates to lifetimes of about  $3 \times 10^{-16}$  sec for the valence holes deep in the band.

The Zn  $M_{2,3}$  SXF spectra show dramatic features with near-threshold excitation. These features can be understood using the second-order perturbation theory for scattering presented in Ref. 42 and the energy-level model of Fig. 14. The process producing the spectra is an elastic Resonant Raman process in which the scattering occurs through a real intermediate state. The electronic excitation producing the energy loss of about 12.4 eV must be from the Zn  $d$  bands located between the upper and lower valence bands and a narrow exciton state located near the conduction-band edge. We note that theory requires that the energy loss is equal to the energy difference between the electron and hole states in the final state of the second-order process, so that the narrow exciton

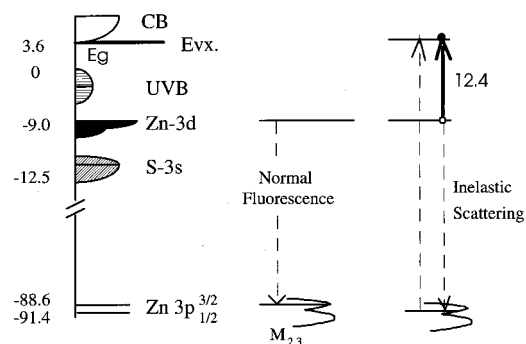


FIG. 14. Schematic diagram of normal fluorescence and electronic resonance Raman processes contributing to photon-excited Zn  $M_{2,3}$  spectra.  $E_g$  denotes the energy gap and  $E_{v,x}$  is the valence exciton.

state is not a core exciton, but a valence exciton in which a hole in the  $d$  band binds an electron in a localized orbital. Because the energy difference is associated with the final state of the scattering process, the width of the observed spectra is not limited by the core-hole lifetime, which broadens the normal fluorescence spectrum. The influence of the core-hole lifetime in the intermediate state does, however, influence the observed spectra by causing the inelastic peak to be modulated according to the intensity of the broad normal fluorescence spectrum. In essence, the energy uncertainty associated with the limited core-hole lifetime allows the resonant inelastic scattering to occur over an energy range consistent with the uncertainty principle.

Several additional features of this example of inelastic scattering deserve comment. The proposed explanation requires that there be a localized exciton state associated with the hole in the  $d$  band. The results presented in Sec. III indicate that exciton effects are not observed in the sulfur  $L$  spectrum. This is consistent with results obtained in other ionic systems, in which localized excitons are found to be associated with the positive-ion but not the negative-ion species. As examples, strong exciton effects are observed in the boron  $K$  spectrum, but not the nitrogen  $K$  spectrum of BN, and are observed in the metal but not the oxygen  $K$  spectra of many oxides. The physical origin of this difference seems to be that the electron density in real space is greater near the negative ion so that holes in inner shells are effectively screened and do not strongly bond local states near the negative ion in ionic solids. In addition to informing us about the physics of coherent processes contributing to fluorescence from solids near threshold, these inelastic-scattering processes provide an alternative means of studying the lowest-energy electronic excitations in solids and especially of the effects of screening on the processes that occur when an additional charge, in the form of a core or valence hole, is introduced into the system.

#### ACKNOWLEDGMENTS

The authors thank D. H. Lowndes of Oak Ridge National Laboratory who provided the ZnS and ZnS<sub>0.5</sub>Se<sub>0.5</sub> samples. This research was supported by National Science Foundation Grants No. DMR-9017997 and No. DMR-9420425. The work was performed at the Advanced Light Source at Lawrence Berkeley National Laboratory, supported by U.S. Department of Energy Contract No. DE-AC03-76SF00098.

- <sup>1</sup>T. Taguchi, Y. Yamada, Y. Endoh, Y. Nozue, J. T. Mullins, T. Ohno, Y. Masumoto, and S. Takada, *Superlatt. Microstruct.* **10**, 207 (1991).
- <sup>2</sup>H. M. Yates, J. O. Williams, and D. J. Cole-Hamilton, *Appl. Phys. Lett.* **59**, 2835 (1991).
- <sup>3</sup>A. Müller and B. Kebs, *Stud. Inorg. Chem.* **5**, 277 (1984).
- <sup>4</sup>N. G. Stoffel, *Phys. Rev. B* **28**, 3306 (1983).
- <sup>5</sup>N. Troullier and José Luís Martins, *Phys. Rev. B* **43**, 1993 (1991).
- <sup>6</sup>J. E. Jaffe, R. Pandey, and M. J. Seel, *Phys. Rev. B* **47**, 6299 (1993).
- <sup>7</sup>J. S. Lin, A. Qteish, M. C. Payne, and V. Heine, *Phys. Rev. B* **47**, 4174 (1993).
- <sup>8</sup>James E. Bernard and Alex Zunger, *Phys. Rev. B* **36**, 3199 (1987).
- <sup>9</sup>Sylvester N. Ekpenuma and Charles W. Myles, *J. Phys. Chem. Solids* **51**, 93 (1990).
- <sup>10</sup>S. I. Kurganskii, O. V. Farberovich, and É. P. Domashevskaya, *Sov. Phys. Semicond.* **14**, 775 (1980); **14**, 837 (1980).
- <sup>11</sup>José Luís Martins, N. Troullier, and S.-H. Wei, *Phys. Rev. B* **43**, 2213 (1991).
- <sup>12</sup>Paul Bendt and Alex Zunger, *Phys. Rev. B* **26**, 3114 (1982).
- <sup>13</sup>Peter Schröer, Peter Krüger, and Johannes Pollmann, *Phys. Rev. B* **47**, 6971 (1993).
- <sup>14</sup>C. S. Wang and B. M. Klein, *Phys. Rev. B* **24**, 3393 (1981).
- <sup>15</sup>Xu Zeng and Meichun Huang, *J. Lumin.* **40&41**, 913 (1988).
- <sup>16</sup>Ming-Zhu Huang and W. Y. Ching, *Phys. Rev. B* **47**, 9449 (1993).
- <sup>17</sup>Oleg Zakharov, Angel Rubio, X. Blase, Marvin L. Cohen, and Steven G. Louie, *Phys. Rev. B* **50**, 10 780 (1994).
- <sup>18</sup>H. Aourag, B. Khelifa, L. Hamerlaine, H. Belarbi, and A. Belaid, *Phys. Lett. A* **145**, 455 (1990).
- <sup>19</sup>Michael Rohlfing, Peter Krüger, and Johannes Pollmann, *Phys. Rev. Lett.* **75**, 3489 (1995).
- <sup>20</sup>Yong-Nian Xu and W. Y. Ching, *Phys. Rev. B* **48**, 4335 (1993).
- <sup>21</sup>Peter Schröer, Peter Krüger, and Johannes Pollmann, *Phys. Rev. B* **48**, 18 264 (1993).
- <sup>22</sup>K. J. Chang, Sverre Froyen, and Marvin L. Cohen, *Phys. Rev. B* **28**, 4736 (1983).
- <sup>23</sup>Akiko Kobayashi, Otto F. Sankey, Stephen M. Volz, and John D. Dow, *Phys. Rev. B* **28**, 935 (1983).
- <sup>24</sup>R. N. Euwema, T. C. Collins, D. G. Shankland, and J. S. DeWitt, *Phys. Rev.* **162**, 710 (1967); T. K. Bergstresser and M. L. Cohen, *ibid.* **164**, 1069 (1967).
- <sup>25</sup>A-I. Ali Dahr and P. M. Lee, *Phys. Scr.* **38**, 441 (1988).
- <sup>26</sup>M. Marychurch and G. C. Morrois, *Surf. Sci.* **154**, L251 (1985).
- <sup>27</sup>Chikara Sugiura, Yasuomi Hayasi, Hiroyosi Konuma, Shigeru Sato, and Makoto Watanabe, *J. Phys. Soc. Jpn.* **29**, 1645 (1970).
- <sup>28</sup>Chikara Sugiura, Yasuomi Hayasi, Hiroyosi Konuma, and Setsuo Kiyono, *J. Phys. Soc. Jpn.* **31**, 1784 (1971).
- <sup>29</sup>K. O. Magnusson, S. A. Flodström, P. Mårtensson, J. M. Nicholls, U. O. Karlsson, R. Engelhardt, and E. E. Koch, *Solid State Commun.* **55**, 643 (1985).
- <sup>30</sup>L. Ley, R. A. Pollak, F. R. McFeely, S. P. Kowalczyk, and D. A. Shirley, *Phys. Rev. B* **9**, 600 (1974).
- <sup>31</sup>C. J. Vesely and D. W. Langer, *Phys. Rev. B* **4**, 451 (1971).
- <sup>32</sup>C. J. Vesely, R. L. Hengehold, and D. W. Langer, *Phys. Rev. B* **5**, 2296 (1972).
- <sup>33</sup>R. L. Hengehold and F. L. Pedrotti, *Phys. Rev. B* **6**, 2262 (1972).
- <sup>34</sup>A. V. Ivanov, L. D. Timakova, and V. N. Kupriyanov, *Opt. Spectrosc.* **31**, 171 (1971); A. V. Ivanov, L. D. Timakova, and V. N. Kupriyanov, *Bull. Acad. Sci. USSR Phys. Ser.* **36**, 251 (1972); **36**, 255 (1972).
- <sup>35</sup>G. Deroubaix and P. Marcus, *Surf. Interface Anal.* **18**, 39 (1992).
- <sup>36</sup>W. L. O'Brien, J. Jia, Q. Y. Dong, T. A. Callcott, K. E. Miyano, D. L. Ederer, D. R. Mueller, and C. C. Kao, *Phys. Rev. Lett.* **70**, 238 (1993).
- <sup>37</sup>J. E. Rubensson, D. Mueller, R. Shuker, D. L. Ederer, C. H. Zhang, J. Jia, and T. A. Callcott, *Phys. Rev. Lett.* **64**, 1047 (1990).
- <sup>38</sup>Y. Ma, N. Wassdahl, P. Skytt, J. Guo, J. Nordgren, P. D. Johnson, J. E. Rubensson, T. Boske, W. Eberhardt, and S. Kevan, *Phys. Rev. Lett.* **69**, 2598 (1992); Y. Ma, *Phys. Rev. B* **49**, 5799 (1994).
- <sup>39</sup>K. E. Miyano, D. L. Ederer, T. A. Callcott, W. L. O'Brien, J. J. Jia, L. Zhou, Q. Y. Dong, Y. Ma, D. C. Woicik, and D. R. Mueller, *Phys. Rev. B* **48**, 1918 (1993).
- <sup>40</sup>J. J. Jia, T. A. Callcott, E. L. Shirley, J. A. Carlisle, L. J. Terminello, A. Asfaw, D. L. Ederer, F. J. Himpsel, and R. C. C. Perera, *Phys. Rev. Lett.* **76**, 4054 (1996).
- <sup>41</sup>J. A. Carlisle, E. L. Shirley, L. J. Terminello, T. A. Callcott, J. J. Jia, D. L. Ederer, R. C. C. Perera, and F. J. Himpsel, *Phys. Rev. Lett.* **74**, 1234 (1995).
- <sup>42</sup>J. Tulkki and T. Åberg, *J. Phys. B* **13**, 3341 (1980); T. Åberg, K. Reinikainen, and O. Keski-Ranhkonen, *Phys. Rev. A* **23**, 153 (1981); J. Tulkki, *ibid.* **27**, 3375 (1983).
- <sup>43</sup>See ALS First Phase Scientific Program No. LBL PUB-706, pp. 11–16, 1992 (unpublished).
- <sup>44</sup>T. A. Callcott, D. L. Ederer, and E. T. Arakawa, *SPIE Proc.* **447**, 61 (1984); T. A. Callcott, C. H. Zhang, K.-L. Tsang, E. T. Arakawa, D. L. Ederer, and J. Kerner, *Nucl. Instrum. Methods Phys. Res. Sect. B* **40&41**, 398 (1989).
- <sup>45</sup>T. A. Callcott, K. L. Tsang, C. H. Zhang, D. L. Ederer, and E. T. Arakawa, *Rev. Sci. Instrum.* **57**, 2680 (1986); T. A. Callcott, K.-L. Tsang, C. H. Zhang, D. L. Ederer, and E. T. Arakawa, *Nucl. Instrum. Methods Phys. Res. Sect. A* **266**, 578 (1988).
- <sup>46</sup>3300 Series MCP/RAE Detector, Quantar Technology, 3004 Mission St., Santa Cruz, CA 95060.
- <sup>47</sup>J. W. McCamy and Douglas H. Lowndes (private communication).
- <sup>48</sup>L. Zhou, T. A. Callcott, and J. J. Jia (unpublished).
- <sup>49</sup>J. C. Fuggle and J. E. Inglesfield, *Top. Appl. Phys.* **69**, 347 (1992).
- <sup>50</sup>Robert B. Leighton, *Principles of Modern Physics* (McGraw-Hill, New York, 1959), p. 228.
- <sup>51</sup>Enrico Clementi and Carlo Rosetti, *At. Data Nucl. Data Tables* **14**, 177 (1974).
- <sup>52</sup>O. Madelung, W. vonder Osten, and U. Rössler, in *Numerical Data and Functional Relationships in Science and Technology*, edited by O. Madelung, Landolt-Börnstein, New Series, Group III, Group 22, Pt. a (Springer-Verlag, Berlin, 1987), pp. 170 and 199.
- <sup>53</sup>N. Wassdahl, J.-E. Rubensson, G. Bray, P. Glans, P. Bleckert, R. Nyholm, S. Cramm, N. Mårtensson, and J. Nordgren, *Phys. Rev. Lett.* **64**, 2807 (1990).
- <sup>54</sup>P. Livins and S. E. Schnatterly, *Phys. Rev. B* **37**, 6731 (1988).